PEDOT:PSS deposition in OECTs: Inkjet printing, aerosol jet printing and spin coating

Giorgia Rinaldi [a,*], Davide Vurro [b], Martina Cicolini [a], Jovana Babic [a], Aris Liboà [b,c], Giuseppe Tarabella [b], Pasquale D'Angelo [b], Simone L. Marasso [a,b], Matteo Cocuzza [a,b], Lorenzo Vigna [a], Fabrizio C. Pirri [a,d], Matteo Parmeggiani [a]

[a] Chilab–Materials and Microsystems Laboratory, Department of Applied Science and Technology (DISAT), Politecnico di Torino, Via Lungo Piazza d'Armi 6, 10034 Turin, Italy
[b] Institute of Materials for Electronics and Magnetism, IMEM-CNR, Parco Area delle Scienze 37/A, 43124 Parma, Italy
[c] Università degli studi di Parma, Str. dell'Università, 12, 43121 Parma, Italy
[d] Center for Sustainable Future Technologies, Italian Institute of Technology, Via Livorno 60, 10144 Turin, Italy

ARTICLE INFO

ABSTRACT

As the world moves towards integrating new functionalities into everyday objects, the demand for diverse substrates grows, making additive manufacturing an invaluable tool. Organic electronic materials have played a major role in this transition thanks to their excellent electronic and mechanical properties, adaptability and solution processability.

The aim of this study is to compare spin coating, inkjet printing (IJP), and aerosol jet printing (AJP) for applying poly(3,4-ethylenedioxythiophene) polystyrene sulfonate (PEDOT:PSS) as the channel material in organic electrochemical transistors (OECTs). This work investigates the often-overlooked impact of deposition techniques on the electrical performance of OECTs. Spin coating has been analysed as a reference technique, while AJP and IJP are addressed as promising pathways towards fully printed OECTs.

The normalized transconductance and I_{on}/I_{off} ratio have been analysed as figures of merit for this study. AJP devices have shown the best performance, displaying a normalized transconductance of 885 S•nm and an I_{on}/I_{off} ratio around 10^3. The spin coated OECTs showed a slightly lower normalized transconductance (740 S•nm) and much lower I_{on}/I_{off} ratio in the order of 10^1. Last, IJP exhibited a transconductance of 433 S•nm and a I_{on}/I_{off} ratio in the order of 10^2.

This work could be beneficial for a wide range of applications, adding an additional degree of freedom to the tunability of the OECT channel properties. It also opens the discussion for more comprehensive studies on the films from a materials perspective.

1. Introduction

As the world approaches a new phase in which new functionalities are integrated into everyday objects, mechanical flexibility, low-cost and large area production have become essential requirements for circuit design. Since silicon technologies are not able to satisfy these needs, additive manufacturing techniques got a foothold in the next generation of electronic devices thanks to their non-contact and digital nature [1]. Organic semiconductors play a major role in this growing industry due to their solution processability and excellent electrical and mechanical properties [2–8].

In the recent years, organic electrochemical transistors (OECTs) have gained significant attention in the fields of protein biosensing [9–12], wearable sensors [13], cell monitoring and whole blood monitoring as well as plant monitoring [14–16], neuromorphic devices [17] and printed logic circuits [18]. First developed by Wrighton et al. in 1984 [19], they have a similar structure to that of organic field-effect transistors (OFETs) [20]. However, while traditional OFETs feature a solid-state dielectric between the gate electrode and the organic semiconductor, OECTs utilize an electrolyte [20], as shown in Fig. 1. Source and drain electrodes, in contact with the organic semiconductor, define the channel of the transistor. Upon the application of a gate voltage ions

---

* Corresponding author.
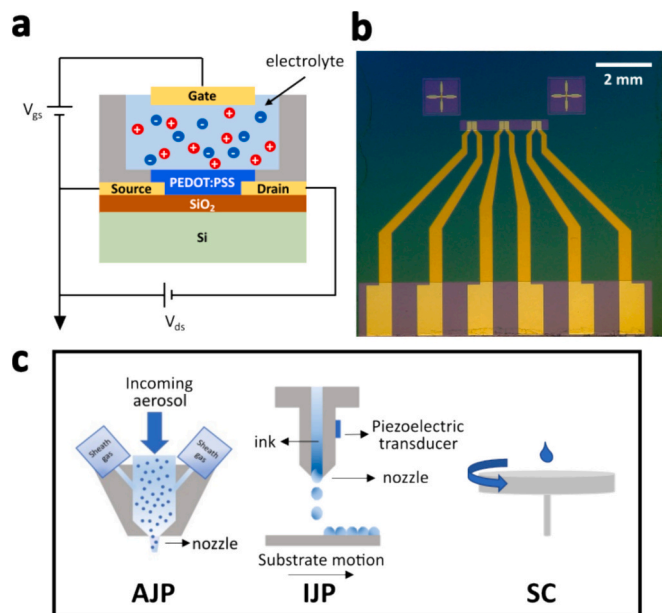E-mail address: giorgia.rinaldi@polito.it (G. Rinaldi).

Fig. 1. (a) Schematic of an OECT device. The figure highlights the organic semiconductor in contact with the liquid electrolyte and the gate electrode immersed into it. (b) Microfabricated chip containing 3 devices before the printing process (c) overview of the deposition techniques used for PEDOT: PSS deposition.

are injected from the electrolyte into the organic semiconductor, changing its doping state and conductivity. While the gate voltage controls the doping state of the film through ion injection, the drain voltage regulates the drain current, which is proportional to the number of mobile charges in the channel [21]. The large capacitance of the electrical double layers and the volumetric contribution of the pseudo-capacitance associated to the permeability to ions of the semiconducting film provide OECTs with a remarkably large gate-channel capacitance [22]. As a result, OECTs are characterised by high transconductance and can operate at low voltages [20]. Another advantage of OECTs over OFETs is the presence of the electrolyte, which eliminates the need for controlled gate-oxide thickness, making them much easier to fabricate [23].

Channel materials for electrochemical transistors require efficient electronic transport as well as easy ion injection to provide high capacitance, therefore they are generally made of organic semiconductors [24,25]. Among them, organic mixed ionic-electronic conductors (OMIECs) are often polymeric materials that support both electronic charge transport along their backbones and ionic (mass) transport through their bulk [24,26]. Consequently, these materials can transduce ionic signals into electronic ones, allowing OECTs to bridge the electronic world and the biological one [21,25,27]. Furthermore, they are biocompatible and have a versatile molecular structure, which leads to tuneable electrical properties [25,26,28].

PEDOT:PSS is a prototypical p-type OMIEC used in OECTs, due to its high hole conductivity and electrochemical stability in aqueous electrolytes, which makes it commercially available as a dispersion for solution processing [2,21,27,29,30].

The ON state of a PEDOT:PSS-based OECT is achieved when the gate voltage is switched OFF and thus holes can hop between the polymeric chains creating a hole current. The sulfonate anions of PSS compensate holes, stabilizing the oxidation state of PEDOT. The gate voltage can be used to modulate the doping state of the polymer. When a positive gate voltage is applied, cations from the electrolyte are injected into the polymer, compensating the PSS anions and causing a dedoping of the OMIEC. The dedoping caused by the injection of the cations is volumetric, as it occurs throughout the volume of the channel [21].

In this study, inkjet printing (IJP), aerosol jet printing (AJP) and spin coating have been compared for the deposition of PEDOT:PSS as OECT channel material, as shown in Fig. 1. Spin coating is the most well-known technique, as it is typically used in silicon technology, and it will be discussed as a reference technique. IJP is the most used printing technique for PEDOT:PSS deposition in OECT fabrication, while AJP is the most recently developed version of jet printing techniques. The latter is an ink-based technique capable of extending the range of printable materials from aqueous to viscous ones (viscosities from 1 cP to 1000 cP) thanks to the two possible atomizers (pneumatic and ultrasonic). AJP is also characterised by an improved resolution compared to IJP, providing printed traces down to a width of 10 μm, and the possibility to print on 3D objects [4].

Previous studies demonstrated the possibility to use IJP [3,6,31,32], AJP [4,8] and spin coating [23,33–36] for the deposition of PEDOT:PSS as channel material in OECTs. In this work, we compare these methods for PEDOT:PSS deposition as channel material for OECTs, successfully highlighting AJP as the technique providing the best results in terms of device performance.

2. Materials and methods

AZ® 1518 positive photoresist, AZ® 400 K developer, Tech-niEtch™ACI2, AZ® 5214 image reversal photoresist, AZ® 726 MIF Developer were purchased from MicroChemicals GmbH. PEDOT:PSS Clevios PH1000 was purchased from Heraus, (3-glycidoxypropyl)tri-methoxysilane (GOPS) was purchased from Alfa Aesar, toluene and acetic acid (ACS reagent grade $\geq$ 99.5%) were purchased from Honey-well. All other chemicals were purchased from Sigma Aldrich and were used as received without further purification. Deionized water was obtained from a reverse osmosis purification (RO) system. Si 4″ wafers finished with a 1 μm thick thermally grown SiO_2 layer were purchased from Si-Mat (Kaufering, Germany) and sued as a substrate for the OECTs.

2.1. Device fabrication

The patterning of the electrodes was carried out in a clean-room facility, following a well-established procedure [37]. Briefly, a 10 nm Ti adhesion layer and a 100 nm Au layer were deposited by electron beam evaporation on a p-type (100) silicon wafer finished with a 1 μm SiO_2 coating, using a ULVAC EBX-14D. Metal pads, interconnects and source/drain contacts were patterned (channel length L = 10 μm, channel width W = 300 μm) by UV-photolithography using AZ® 1518 positive photoresist, exposed in a NEUTRONIX QUINTEL NXQ-4006 Mask Aligner and developed using AZ® 400 K Developer:DI-H_2O = 1:3. Wet etching was then performed using a solution of HF:H_2O_2:DI-H_2O = 1:1:20 for titanium and TechniEtch™ACI2 for gold. A 150 μm Al_2O_3 passivation layer was patterned via a lift-off process: photolithography was carried out using AZ® 5214 image reversal photoresist, exposed in the mask aligner and developed in pure AZ® MIF 726 Developer. Lift-off in dimethyl sulfoxide (DMSO) was then finalized.

A 22 mM (3-glycidoxypropyl)trimethoxysilane (GOPS) solution in toluene:acetic acid = 200:1 v/v was deposited on the chips as adhesion promoter for PEDOT:PSS channel material. The solution was spin-coated on the chips (4000 rpm, 60 s) and then baked on a hot plate at 120 °C for 30 s.

PEDOT:PSS deposition is carried out outside the cleanroom by IJP and AJP. The PEDOT:PSS ink solution contained 76% v/v Clevios PH1000, 19% v/v ethylene glycol to enhance PEDOT:PSS conductivity, 4% v/v dodecylbenzenesulfonic acid (DBSA) as a surfactant and 1% GOPS to enhance stability in polar solvents.

The ink was filtered with a 0.22 μm syringe filter and then deposited by spin coating, AJP or IJP. The spin coating process was carried out at 1000 rpm for 30 s. The process was repeated 10 times to achieve the desired thickness, drying the film on a hot plate for 1 min at 110 °C after

the deposition of every layer. IJP was achieved by a piezoelectric drop-on-demand Jetlab®4 (Microfab technologies) with a 50 μm nozzle diameter and AJP by Aerosol Jet® 200 Series (OPTOMEC) with a 200 μm nozzle diameter and an ultrasonic atomizer. The IJP process was performed using fly velocity of 25 mm/s, distance from feature borders of 1 μm and spacing between drops of 40 μm. AJP was instead carried out with a flow velocity of 2 mm/s, overlapping of 20/30%, a focusing ratio (FR) of 1.4 with a sheath gas pressure of 35 SCCM and carrier gas pressure of 25 sccm. During the aerosol deposition the plate temperature and ultrasonic current are respectively set to 60 °C and 0.5 mA. The PEDOT:PSS ink used for AJP deposition was diluted 1:1 *v*/v with deionized water to achieve the desired viscosity (range 1–10 cP for ultrasonic atomizers).

The printed samples (AJP and IJP) were baked on a hot plate (120 °C, 15 min) to let the solvents evaporate and all the samples (IJP, AJP and spin coating) were then annealed in the oven (150 °C, 30 min) in order to improve conduction and stability.

2.2. Electrical characterisation

The devices were characterised with Keysight B2912A Precision Source/Measure Unit using a Ag/AgCl gate electrode. Each measurement is repeated at four different scan rates (9.76 mV/s, 19.51 mV/s, 97.56 mV/s, 195.12 mV/s). Output characteristics were acquired for a gate voltage of −0.2 V and a drain voltage between −0.6 V and 0.0 V. Transcharacteristics were performed for 3 cycles (last one selected in the measurements shown) at a drain voltage of −0.2 V and a gate voltage ranging between −0.2 V and 0.6 V. All measurements were carried out using NaCl 0.1 M as electrolyte and polydimethylsiloxane (PDMS) wells to confine it on the channel. Device transconductance g_m, defined as $\frac{dI_{DS}}{dV_G}$, has been calculated from the transfer characteristics to provide its peak value $g_{m,max}$ which corresponds to the maximum transconductance.

2.3. Physical characterisation

The scanning probe microscopy (SEM) images were performed with ZEISS Supra 40 Field Emission Scanning Electron Microscope and FEI Inspect F, while atomic force microscopy (AFM) data were obtained with Oxford Instruments MFP-3D Origin. The SEM images were obtained using a voltage of 5 kV and 10 kV and an aperture of 30 μm. Differently, the AFM images were collected in tapping mode using a tip AC160 for tapping mode.

3. Results and discussion

In this section we perform a characterisation of the three sets of devices in order to assess which deposition technique yields the best results with PEDOT:PSS-based devices, based on their electrical performance. Electrical characterisation was initially performed to assess the steady state behaviour of the devices. Eventually, a physical characerisation was carried out to better understand the working principle of the devices and to justify their electrical performance.

Before conducting the electrical measurements, thorough thickness characterisation was carried out, with a focus on printed devices. This necessity comes from the thickness dependence of the drain current expressed in the Bernard's model [38].

The deposition parameters were then selected to match the thickness of ~~AJP and IJP devices~~ the AJP, IJP and spin coated films. In particular, the PEDOT:PSS films were deposited to achieve a thickness around 1.5 μm. The thickness has been chosen to be in the micrometre range to enable the deposition of conformal films with the AJP technique, which typically produces lower quality films compared to the other two techniques. Both spin-coating and IJP techniques can deposit high quality films in the nanometre range.

The output and transfer characteristics were measured for 4 different

scan rates for the 3 sets of devices, as can be seen in Fig. 2. Among the deposition techniques analysed, spin coated devices have been found to have the best ON current −9.5 ± 0.9 mA) followed by AJP (−8.0 ± 0.5 mA) and IJP (−4.8 ± 0.6 mA).

Fig. 3a and b contain information on the transconductance achieved by the different sets of devices. Transconductance represents the voltage-current amplification of an OECT and it depends both on channel geometry and biasing conditions [24]. The peak transconductance value $g_{m,max}$ was normalized in Fig. 3a to account for the geometric parameters of the devices; specifically it was multiplied by the factor $d \bullet W/L$ where d is the thickness of the film, W and L are the width and length of the channel respectively. The normalized transconductance peak value provided by AJP devices reached a value around 885.1 ± 51.5 S•nm, showing the best amplification. Although the spin coated devices achieved the highest ON current, they exhibited a normalized maximum transconductance of 740.9 ± 79.6 S•nm. The IJP devices have lower normalized maximum transconductance, namely 433.0 ± 36.7 S•nm. Further analysis revealed that the transconductance does not change with the scan rate, indicating clear stability.

The results shown in Fig. 3c and d provide a deeper understanding of the switching performance of the devices. Fig. 3d compares the performance of the different devices on a semi-logarithmic plot of the modulus of the drain current with respect to the gate voltage. As can be observed, AJP devices reach the lowest OFF current regardless of their high ON current. As shown in Fig. 3c, their I_{on}/I_{off} ratio was found to be 3576.6 ± 921.2, approximately 6.5 times higher than IJP devices. The ratio for IJP devices was indeed 542.4 ± 45.3, while the one for spin coated devices has been computed to be 55.2 ± 45.0. This is an interesting result considering that, in principle, the device becomes slower as the channel thickness increases [[20]]. However, the devices under analysis have similar thickness values, making the switching speed independent of this parameter.

An interpretation of these results can be provided analysing the physical characterisation of the printed devices. The SEM images provided in Fig. 4 show that the AJP devices ~~have~~ exhibit a morphology exposing a larger area compared to the IJP and spin coated films. These findings are supported by the AFM measurements, which show a significantly higher roughness in AJP films. In particular, the root mean square (RMS) roughness found for the AJP films was found to be 40.1 nm, whereas the one for the IJP films was only 4.6 nm. Previous works have addressed the surface roughness of spin coated films and found their RMS value to saturate around 5 nm for films thicker than 70 nm, similarly to the IJP films [39]. The higher exposed surface area and surface to volume ratio of the AJP PEDOT:PSS channels might favour ion diffusion within the film, allowing for a better and faster volumetric doping of the film, as similarly showed for other polymers [40].

Overall, these results suggest that AJP might be the best option among those considered for the deposition of PEDOT:PSS as a channel material for OECT devices.

Additional research is warranted to elucidate the conduction mechanisms within the films, as further microstructural characterizations might help to explain structural/property relationships that account for the different transport properties. The variation in the performance may be attributed to the morphostructure of the PEDOT:PSS films, which is known to undergo alterations with different deposition techniques [41].

4. Conclusions

In this paper AJP, IJP and spin coating have been compared as PEDOT:PSS deposition methods for OECTs channels. The analysis performed successfully identifies AJP as the most promising technique for the highlighted purpose.

Electrical characterizations of the devices have been carried out showing that AJP devices outperformed both IJP and spin coated ones in terms of amplification and switching behaviour, providing the highest
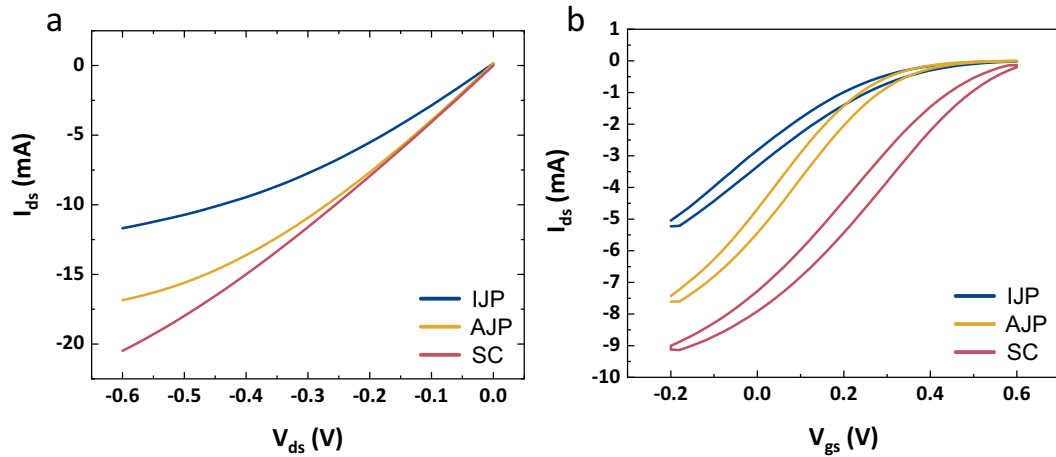
Fig. 2. Electrical characterisation of the devices. (a) output characteristics for $V_{gs} = -0.2$ V (b) transcharacteristics for $V_{ds} = -0.2$ V.
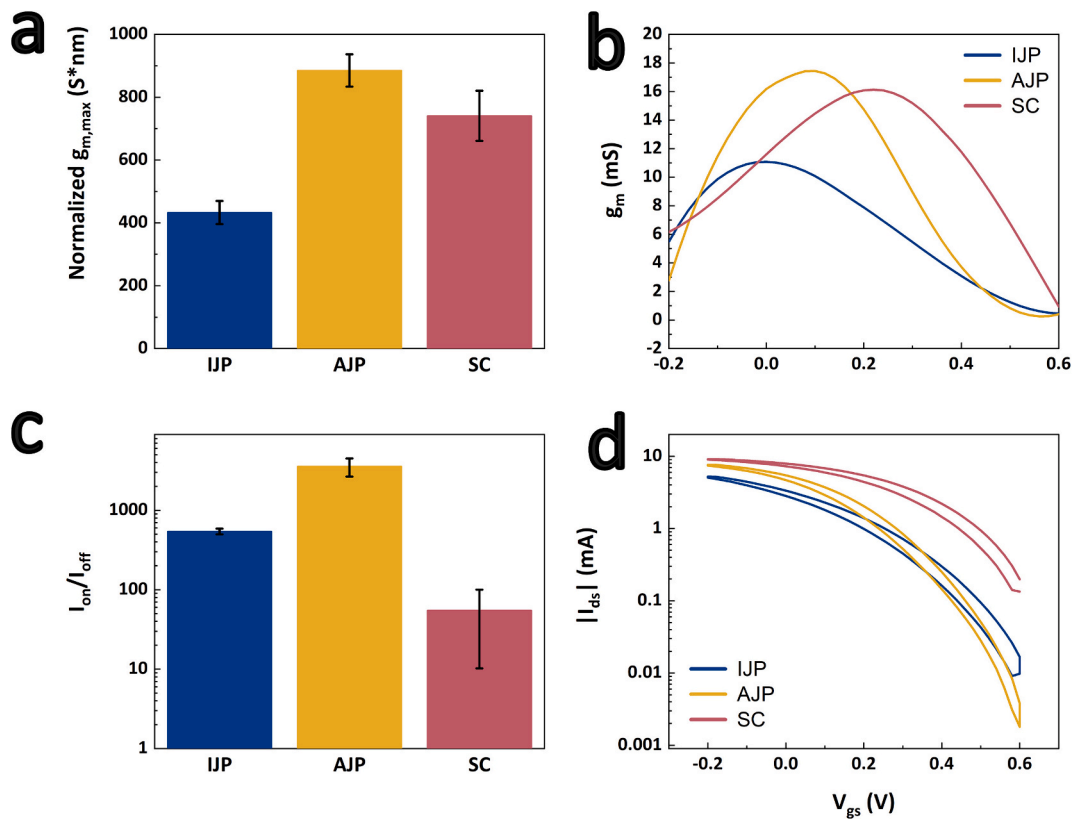

Fig. 3. (a) Histogram of the maximum transconductance normalized by the product d*W/L, (b) Transconductance curves, (c) Histogram of the Ion/Ioff ratio in a semi-logarithmic scale, (d) semi-logarithmic plot of the modulus of the drain current for the different deposition techniques analysed.

maximum transconductance and I_{on}/I_{off} ratio. These results were partially corroborated by the physical characterisation, which proved the AJP devices to have a higher surface roughness and, as a consequence, to be more open to ion injection. Further characterisation is needed to clarify structural/property relationships for the different deposition techniques.

Although additive manufacturing is a valid alternative to spin coating, it also presents additional challenges such as process control and resolution. While additive manufacturing provides faster and easier fabrication, spin coating can take advantage of the well-established lithographic processes to achieve a higher level of control, reproducibility, and feature resolution. Furthermore, AJP is optimally suited for

thicker films, which consequently limits its range of applications.

Future studies will address the morphostructure of PEDOT:PSS films deposited using different techniques and the ionic transport within these films. This aims to deepen our understanding of their impact on OECT performance, thereby leveraging distinct methods for specific applications. This study also paves the way to exploring the application of AJP PEDOT:PSS-based OECTs in the field of biosensing, taking advantage of their high g_m and I_{on}/I_{off} ratio to achieve increasingly lower limits of detection.
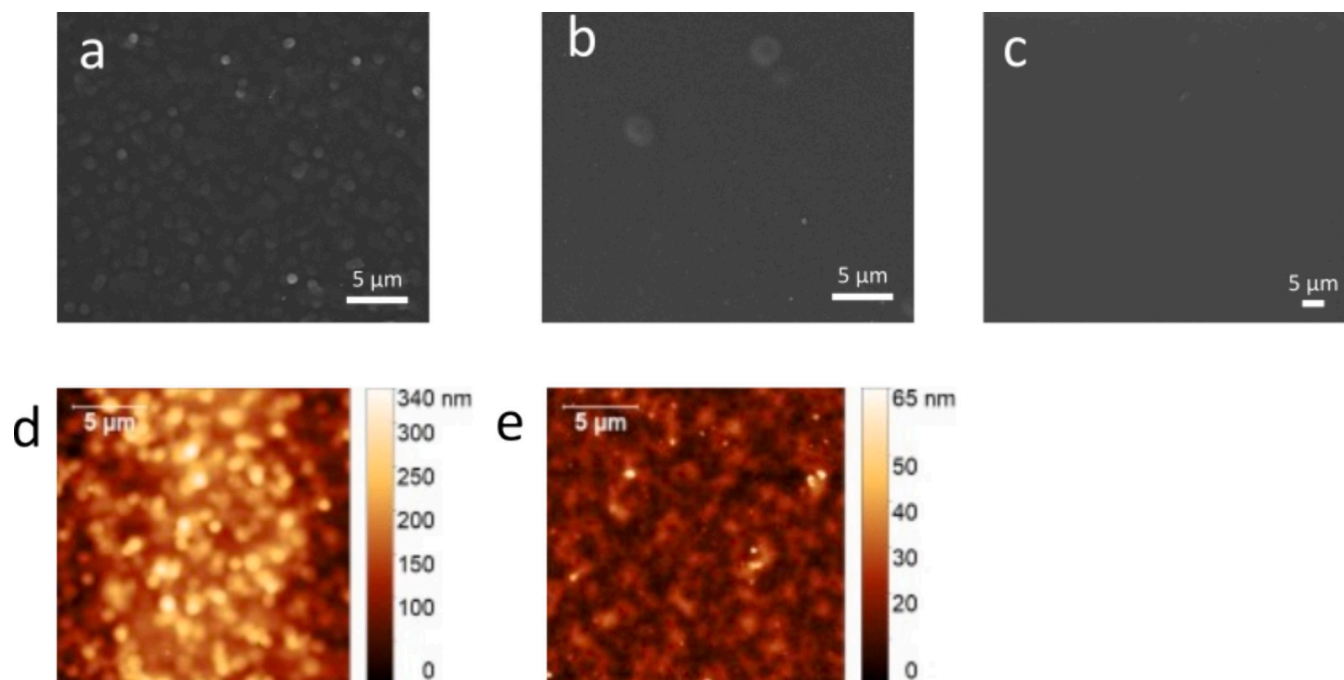
Fig. 4. Physical characterisation of the printed films. SEM characterisation of the (a) IJP and (b) AJP films. AFM characterisation of the (a) IJP and (b) AJP films.

Declaration of competing interest

The authors declare that they have no known competing financial interests or personal relationships that could have appeared to influence the work reported in this paper.

Data availability

Data will be made available on request.

Acknowledgements

References

[1] S.L. Marasso, M. Cocuzza (Eds.), High Resolution Manufacturing from 2D to 3D/4D Printing, Springer International Publishing, Cham, 2022.
[2] F. Torricelli, D.Z. Adrahtas, Z. Bao, M. Berggren, F. Biscarini, A. Bonfiglio, C. A. Bortolotti, C.D. Frisbie, E. Macchia, G.G. Malliaras, I. McCulloch, M. Moser, T. Q. Nguyen, R.M. Owens, A. Salleo, A. Spanu, L. Torsi, Nat Rev Methods Primers (2021) 1, https://doi.org/10.1038/s43586-021-00065-8.
[3] S. Demuru, C.H. Huang, K. Parvez, R. Worsley, G. Mattana, B. Piro, V. Noël, C. Casiraghi, D. Briand, ACS Appl Nano Mater 5 (2022) 1664.
[4] G. Tarabella, D. Vurro, S. Lai, P. D'Angelo, L. Ascari, S. Iannotta, Flexible and Printed Electronics 5 (2020) 014005.
[5] G. Mattana, A. Loi, M. Woytasik, M. Barbaro, V. Noël, B. Piro, Adv Mater Technol 2 (2017) 1700063.
[6] R. Mannerbro, M. Ranlöf, N. Robinson, R. Forchheimer, Synth. Met. 158 (2008) 556.
[7] A. Makhinia, K. Hübscher, V. Beni, P. Andersson Ersman, *Adv* Mater. Technol. 2022, 7, 2200153.
[8] J. Fan, A.A. Forero Pico, M. Gupta, Mater Adv 2 (2021) 7445.
[9] S. Khan, S. Ali, A. Khan, B. Wang, A. Bermak, IEEE Sensors J. 21 (2021) 4167.
[10] M. Barra, G. Tomaiuolo, V.R. Villella, S. Esposito, A. Liboà, P. D'Angelo, S. L. Marasso, M. Cocuzza, V. Bertana, E. Camilli, V. Preziosi, Biosensors (Basel) 13 (2023) 739.
[11] V. Preziosi, M. Barra, V.R. Villella, S. Esposito, P. D'Angelo, S.L. Marasso, M. Cocuzza, A. Cassinese, S. Guido, Biosensors (Basel) 13 (2023) 448.
[12] V. Bertana, G. Scordo, M. Parmeggiani, L. Scaltrito, S. Ferrero, M.G. Gomez, M. Cocuzza, D. Vurro, P. D'Angelo, S. Iannotta, C.F. Pirri, S.L. Marasso, Sci. Rep. 10 (2020) 13335.
[13] S.T. Keene, D. Fogarty, R. Cooke, C.D. Casadevall, A. Salleo, O. Parlak, Adv. Healthc. Mater. 8 (2019) 1901321.
[14] C. Nicolò, M. Parmeggiani, S. Villata, D. Baruffaldi, S.L. Marasso, G. Canavese, M. Cocuzza, C.F. Pirri, F. Frascella, Micro and Nano Engineering 16 (2022) 100147.
[15] V. Preziosi, M. Barra, G. Tomaiuolo, P. D'Angelo, S.L. Marasso, A. Verna, M. Cocuzza, A. Cassinese, S. Guido, J. Mater. Chem. B 10 (2022) 87.
[16] F. Gentile, F. Vurro, M. Janni, R. Manfredi, F. Cellini, A. Petrozza, A. Zappettini, N. Coppedè, Adv Electron Mater (2022) 8, https://doi.org/10.1002/aelm.202200092.
[17] H. Ling, D.A. Koutsouras, S. Kazemzadeh, Y. Van De Burgt, F. Yan, P. Gkoupidenis, Appl. Phys. Rev. (2020) 7, https://doi.org/10.1063/1.5122249.
[18] H. Sun, M. Vagin, S. Wang, X. Crispin, R. Forchheimer, M. Berggren, S. Fabiano, H. Sun, M. Vagin, S. Wang, X. Crispin, M. Berggren, S. Fabiano, R. Forchheimer, Adv. Mater. 30 (2018) 1704916.
[19] H.S. White, G.P. Kittlesen, M.S. Wrighton, J. Am. Chem. Soc. 106 (1984) 5375.
[20] J.T. Friedlein, R.R. McLeod, J. Rivnay, Org. Electron. 63 (2018) 398.
[21] J. Rivnay, S. Inal, A. Salleo, R.M. Owens, M. Berggren, G.G. Malliaras, Nat. Rev. Mater. 3 (2018) 17086.
[22] P. D'Angelo, S.L. Marasso, A. Verna, A. Ballesio, M. Parmeggiani, A. Sanginario, G. Tarabella, D. Demarchi, C.F. Pirri, M. Cocuzza, S. Iannotta, Small (2019) 15, https://doi.org/10.1002/smll.201902332.
[23] J. Rivnay, P. Leleux, M. Sessolo, D. Khodagholy, T. Hervé, M. Fiocchi, G. G. Malliaras, Adv. Mater. 25 (2013) 7010.
[24] S. Inal, G.G. Malliaras, J. Rivnay, Nat. Commun. 8 (1) (2017).
[25] M. Parmeggiani, A. Ballesio, S. Battistoni, R. Carcione, M. Cocuzza, P. D'Angelo, V. V. Erokhin, S.L. Marasso, G. Rinaldi, G. Tarabella, D. Vurro, C.F. Pirri, Micromachines (Basel) (2023) 14, https://doi.org/10.3390/mi14020460.
[26] M. Asplund, T. Nyberg, O. Inganäs, Polym. Chem. 1 (2010) 1374.
[27] C.B. Nielsen, A. Giovannitti, D.T. Sbircea, E. Bandiello, M.R. Niazi, D.A. Hanifi, M. Sessolo, A. Amassian, G.G. Malliaras, J. Rivnay, I. McCulloch, J. Am. Chem. Soc. 138 (2016) 10252.
[28] Y. Wang, C. Zhu, R. Pfattner, H. Yan, L. Jin, S. Chen, F. Molina-Lopez, F. Lissel, J. Liu, N.I. Rabiah, Z. Chen, J.W. Chung, C. Linder, M.F. Toney, B. Murmann, Z. Bao, Sci. Adv. (2017) 3, https://doi.org/10.1126/SCIADV.1602076/SUPPL_FILE/1602076_VIDEOS3.MOV.
[29] J. Rivnay, S. Inal, B.A. Collins, M. Sessolo, E. Stavrinidou, X. Strakosas, C. Tassone, D.M. Delongchamp, G.G. Malliaras, Nat. Commun. 7 (1) (2016).
[30] A. Elschner, S. Kirchmeyer, W. Lövenich, U. Merker, K. Reuter, PEDOT: principles and applications of an intrinsically conductive, Polymer 1 (2010).
[31] L. Basiricò, P. Cosseddu, B. Fraboni, A. Bonfiglio, Thin Solid Films 520 (2011) 1291.

[32] E. Bihar, Y. Deng, T. Miyake, M. Saadaoui, G.G. Malliaras, M. Rolandi, Sci. Rep. 6 (1) (2016).

[33] H. Tang, F. Yan, P. Lin, J. Xu, H.L.W. Chan, Adv. Funct. Mater. 21 (2011) 2264.

[34] M. Braendlein, A.M. Pappa, M. Ferro, A. Lopresti, C. Acquaviva, E. Mamessier, G. G. Malliaras, R.M. Owens, Adv. Mater. 29 (2017), https://doi.org/10.1002/adma.201605744.

[35] D. Gentili, P. D'Angelo, F. Militano, R. Mazzei, T. Poerio, M. Brucale, G. Tarabella, S. Bonetti, S.L. Marasso, M. Cocuzza, L. Giorno, S. Iannotta, M. Cavallini, J. Mater. Chem. B 6 (2018) 5400.

[36] Q. Thiburce, N. Melosh, A. Salleo, Flexible and Printed Electronics 7 (2022), https://doi.org/10.1088/2058-8585/ac808a.

[37] M. Segantini, A. Ballesio, G. Palmara, P. Zaccagnini, F. Frascella, G. Garzone, S. L. Marasso, M. Cocuzza, M. Parmeggiani, Adv Electron Mater 8 (2022), https://doi.org/10.1002/aelm.202101332.

[38] D.A. Bernards, G.G. Malliaras, Adv. Funct. Mater. 17 (2007) 3538.

[39] P. D'Angelo, G. Tarabella, A. Romeo, S.L. Marasso, A. Verna, M. Cocuzza, C. Peruzzi, D. Vurro, S. Iannotta, Materials 12 (2018), https://doi.org/10.3390/ma12010009.

[40] R. Sajapin, D. Vurro, P. D'Angelo, G. Tarabella, S.L. Marasso, M. Cocuzza, M. Botti, M. Buttrini, A. Calderaro, T. Berzina, S. Iannotta, ACS Appl. Electron. Mater. 4 (2022) 5875.

[41] P. Wilson, C. Lei, C. Lekakou, J.F. Watts, Org. Electron. 15 (2014) 2043.